Macrocyclic $[Cu^{I/II}(bite)]^{+/2+}$ (bite = biphenyldiimino dithioether): An Example of Fully-Gated Electron Transfer and Its Biological Relevance[1]

Scott Flanagan,[†] Jun Dong,[‡] Kenneth Haller,[§] Shengke Wang,[‡] W. Robert Scheidt,*[,§] Robert A. Scott,*[,‡] Thomas R. Webb,*[,∥] David M. Stanbury,*[,∥] and Lon J. Wilson*[,†]

Contribution from the Department of Chemistry and Laboratory for Biochemical and Genetic Engineering MS-60, William Marsh Rice University, 6100 Main Street, Houston, Texas 77005-1892, the Department of Chemistry and Biochemistry, University of Notre Dame, Notre Dame, Indiana 46556, the Center for Metalloenzyme Studies, University of Georgia, Athens, Georgia 30602-2556, and the Department of Chemistry, Auburn University, Auburn, Alabama 36849

Received December 23, 1996[⊗]

Abstract: Template condensation of 2,2′-diaminobiphenyl, 1,4-bis(2-formylphenyl)-1,4-dithiabutane, and copper(II) tetrafluoroborate yields the new macrocyclic compound $[Cu^{I}(bite)](BF_4)$ (bite = biphenyldiimino dithioether). $[Cu^{I}(bite)]BF_4$ crystallizes in the orthorhombic space group $P2_12_12_1$ with $a = 14.379(3)$ Å, $b = 21.370(3)$ Å, $c = 8.046(2)$ Å, $V = 2534.7(7)$ Å^3, $Z = 4$, $R_1 = 0.045$, and $R_2 = 0.048$. The X-ray structure of $[Cu^{I}(bite)](BF_4)$ reveals distorted tetrahedral N_2S_2 coordination about copper, with one unusually short Cu−S(thioether) bond of 2.194(2) Å. Oxidation of $[Cu^{I}(bite)](BF_4)$ with nitrosyl tetrafluoroborate gives $[Cu^{II}(bite)](BF_4)_2$. $[Cu^{II}(bite)](BF_4)_2$ crystallizes in the tetragonal space group $I4_1/a$ with $a = 11.640(2)$ Å, $c = 39.527(3)$ Å, $V = 5355.6(7)$ Å^3, $Z = 8$, $R_1 = 0.061$, and $R_2 = 0.063$. X-ray crystallography of $[Cu^{II}(bite)](BF_4)_2$ reveals an approximately square planar CuN_2S_2 structure with two distant axial BF_4^- anions (Cu−F 2.546(4) Å) completing a "pseudo-octahedral" coordination sphere. Comparative EXAFS studies of solid samples and acetonitrile solutions of $[Cu^{I}(bite)](BF_4)$ and $[Cu^{II}(bite)](BF_4)_2$ demonstrate that the primary coordination environments of both species are the same in solution as in the solid. Copper(I/II) electron self-exchange kinetics measured by ^{1}H NMR line broadening of $[Cu^{I}(bite)]^+$ in the presence of $[Cu^{II}(bite)]^{2+}$ reveal an overall *first-order* process with a rate constant of 21.7(1.9) s^{-1} at 295 K in acetone-d_6. This result represents the first example of fully-gated electron transfer by small-molecule copper(I). The gating process likely involves inversion at sulfur and the tetrahedral → square planar structural change coincident with electron transfer. Variable-temperature ^{1}H NMR coalescence temperatures for methylene ligand protons of $[Cu^{I}(bite)](BF_4)$ (287 K) demonstrate possible correlation of fast electron transfer with high ligand mobility for this and related small-molecule copper(I/II) couples. Comparison with other small-molecule copper systems also reveals that fast electron transfer is not always observed with coordination-number-invariance and conserved geometry during redox turnover, contrary to popular interpretations of the entatic state hypothesis for blue-copper protein active sites.

Introduction

Unlike heme iron and iron−sulfur electron-transfer proteins, cuproproteins have no extrudable coordination complex, since the active-site structure exists only through chelation of the copper ion with protein residues.[2] Studies carried out on the proteins themselves are severely limited due to factors such as the restricted range of temperatures and solvents that the native protein can endure. Furthermore, when results can be obtained from large biomolecules, interpretation of the data is hampered by difficulties in distinguishing properties of the active site from properties of the protein as a whole. Thus, the study of small-molecule copper complexes offers one of the few means to evaluate the active-site contribution to electron transfer for copper proteins. Small-molecule model compounds for copper protein electron-transfer dynamics should ideally demonstrate coordination-number-invariance (CNI) and an outer-sphere mechanism of electron transfer. *Synthetic copper systems rarely meet these two criteria*, and the literature documents only a few well-defined candidates.[3−14] The high kinetic lability of copper and its tendency to adopt different coordination numbers and

[†] Rice University.
[‡] University of Georgia.
[§] University of Notre Dame.
[∥] Auburn University.

[⊗] Abstract published in *Advance ACS Abstracts,* August 15, 1997.

(1) Taken in part from the following: Flanagan, J. S. Ph.D. Dissertation, Rice University, 1995.

(2) Solomon, E. I. In *Copper Coordination Chemistry: Biological & Inorganic Perspectives*; Karlin, K. D., Zubieta, J., Eds.; Adenine Press: Guilderland, New York, 1983; pp 1−22.

(3) Coggin, D. K.; González, J. A.; Kook, A. M.; Stanbury, D. M.; Wilson, L. J. *Inorg. Chem.* **1991**, *30*, 1115−1125.

(4) Coggin, D. K.; González, J. A.; Kook, A. M.; Bergman, C.; Brennan, T. D.; Scheidt, W. R.; Stanbury, D. M.; Wilson, L. J. *Inorg. Chem.* **1991**, *30*, 1125−1134.

(5) Knapp, S.; Keenan, T. P.; Zhang, X.; Fikar, R.; Potenza, J. A.; Schugar, H. J. *J. Am. Chem. Soc.* **1987**, *109*, 1882.

(6) Knapp, S.; Keenan, T. P.; Liu, J.; Potenza, J. A.; Schugar, H. J. *Inorg. Chem.* **1990**, *29*, 2191.

(7) Knapp, S.; Keenan, T. P.; Zhang, X.; Fikar, R.; Potenza, J. A.; Schugar, H. J. *J. Am. Chem. Soc.* **1990**, *112*, 3452−3464.

(8) Groenveld, C. M.; van Rijn, J.; Reedijk, J.; Canters, G. W. *J. Am. Chem. Soc.* **1988**, *110*, 4893−4900.

(9) Drew, M. G. B.; Cairns, C.; McFall, S. G.; Nelson, S. M. *J. Chem. Soc., Dalton Trans.* **1980**, 2020−2027.

(10) Drew, M. G. B.; Cairns, C.; Nelson, S. M.; Nelson, J. *J. Chem. Soc., Dalton Trans.* **1981**, 942−948.

(11) Goodwin, J. A.; Bodager, G. A.; Wilson, L. J.; Stanbury, D. M.; Scheidt, W. R. *Inorg. Chem.* **1989**, *28*, 35.

(12) Goodwin, J. A.; Stanbury, D. M.; Wilson, L. J.; Eigenbrot, C. W.; Schiedt, W. R. *Inorg. Chem.* **1987**, *109*, 2979−2991.

S0002-7863(96)04403-4 CCC: $14.00

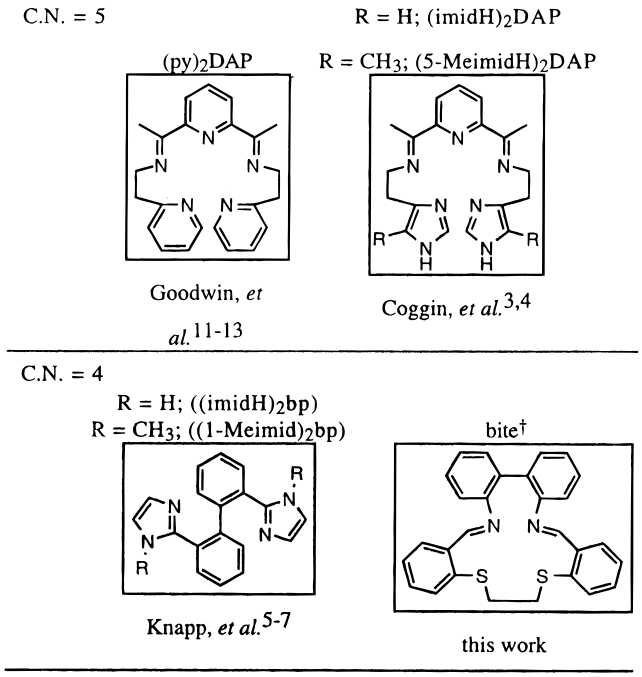

Figure 1. Ligands for the CNI copper compounds.

geometries in the +1 and +2 oxidation states pose formidable obstacles in the design and synthesis of appropriate small-molecule systems. Despite such difficulties, the present work describes kinetics results for a new four-coordinate copper couple, $[Cu^{I/II}(bite)]^{+/2+}$, by employing a ligand carefully tailored to control such problems (Figure 1). The present data supplement those collected for several previously described open-chain five-coordinate complexes,[3,4,11−13] while being the first to be obtained for a closed, macrocyclic ligand designed to enforce an outer-sphere electron self-exchange reaction mechanism.

Experimental Section

Materials. All materials were used as received unless otherwise noted. Acetone, dichloromethane, chloroform, diethyl ether, concentrated aqueous hydrochloric acid, potassium hydroxide, methanol, sodium sulfate (anhydrous), concentrated aqueous ammonia, and tetrahydrofuran were obtained from EM Science. Diatomaceous earth (Celite), 2,2′-dinitrobiphenyl, 1,2-dibromoethane, lithium aluminum hydride, manganese dioxide (activated), sodium tetrafluoroborate, nitroethane, silica gel, tin(II) chloride (anhydrous), thiosalicylic acid, and tetrabutylammonium tetrafluoroborate were obtained from Aldrich. Argon and nitrogen were obtained from Trigas Industrial Gases. Chloroform-d_6, acetonitrile-d_3, and acetone-d_6 were obtained from Cambridge Isotope Laboratories. Copper(II) tetrafluoroborate tetrahydrate was obtained from Alfa. Copper(II) sulfate, *n*-butanol, and potassium chloride were obtained from J. T. Baker. Ethanol was obtained from Quantum Chemical Corporation. Nitrosyl tetrafluoroborate was obtained from Strem.

2,2′-Diaminobiphenyl. 2,2′-Dinitrobiphenyl (10.05 g) was dissolved in ∼500 mL of concentrated aqueous HCl. Anhydrous $SnCl_2$ (64.83 g) was mixed with 5 mL of deionized water and added to the HCl solution. Stirring the mixture for 30 min resulted in a cloudy pale yellow solution. The temperature was then brought to between 65 and 70 °C and held there for 30 min. During heating, the solution became darker yellow. The temperature was reduced to 5 °C by means of an ice bath, and the mixture was slowly neutralized with 300 mL of cold concentrated aqueous NH_3. The now basic solution was brought to neutrality by the addition of 20 mL of HCl. The mixture appeared as a milk-white suspension. Dichloromethane (500 mL) was added, and the resulting mixture was stirred for ∼30 min. The CH_2Cl_2 layer was saved. The inorganic phase was washed twice more with 200 mL portions of CH_2Cl_2. The combined organic fractions were washed four times with 150 mL portions of deionized water, dried with Na_2SO_4 (anhydrous), and evaporated to dryness to yield an orange oil. The oil was left under vacuum overnight, yielding 7.94 g of crude product. It was then triturated with 1 mL of ethanol to yield a mass of yellow solid. The collected solid was dissolved in ∼20 mL of hot ethanol. After the solution was cooled in a freezer for ∼15 min, a batch of yellow-orange crystals was collected and determined to be unreacted 2,2′-dinitrobiphenyl. The ethanol solution was then left to cool overnight in the freezer, yielding pure, pale yellow crystals of 2,2′-diaminobiphenyl. The final product was dried overnight under vacuum. Yield: 5.47 g (72%), mp 77−79 °C (lit.[15] 80 °C). ^{1}H NMR (90 MHz, TMS internal reference at 0 ppm, $CDCl_3$): δ 6.70−7.67 (8H, m, biphenyl), 3.70 (4H, m, -NH_2, br).

1,4-Bis(2-carboxyphenyl)-1,4-dithiabutane. 1,4-Bis(2-carboxyphenyl)-1,4-dithiabutane was prepared by the method of Livingstone, with minor modification.[16] A mixture of 8 g of KOH, 10 g of thiosalicylic acid, 6.1 g of 1,2-dibromoethane, and 250 mL of ethanol was brought to reflux under N_2 for 1.5 h. The resultant cloudy brown solution was poured into ∼200 mL of deionized water. The mixture immediately turned clear brown. The addition of ∼50 mL of concentrated aqueous HCl resulted in the precipitation of a fine white powder. The mixture was allowed to stand overnight, whereupon the solid was collected by Büchner filtration and rinsed well with hot deionized water, methanol, acetone, and finally diethyl ether. The filter cake was dried in a vacuum desiccator (10^{-3} Torr) for 30 min. The still-moist product was suspended in 250 mL of 50/50 methanol/CH_2Cl_2 and refiltered. The filter cake was placed back in the vacuum desiccator and left overnight. The low solubility of the product in any solvent except pyridine precluded characterization by conventional ^{1}H NMR. The success of all subsequent synthetic steps and eventual characterization of the final products by X-ray crystallography serve as proof of the identity of the compound. Yield: 18.3 g (84%), mp 291−295 °C (lit.[16] 297 °C).

1,4-Bis(2-(hydroxymethyl)phenyl)-1,4-dithiabutane. The procedure of Lindoy and Smith[17] for the synthesis of 1,4-bis(2-(hydroxymethyl)phenyl)-1,4-dithiabutane was modified to give improved yield. 1,4-Bis(2-carboxyphenyl)-1,4-dithiabutane (45.53 g) was added to 500 mL of dry tetrahydrofuran (THF, freshly distilled from lithium aluminum hydride (LAH)). LAH (11.37 g) was added carefully in small portions. The addition of LAH released enough heat to bring the THF to boiling. At this point, the round-bottomed flask containing the mixture was fitted with a reflux condenser, and the round-bottomed flask was suspended in a heated ultrasonic bath (65 °C) overnight. The next day, the gray suspension was cautiously poured into 500 mL of methanol to produce vigorous bubbling. Deionized water was then carefully added over a period of 45 min producing a white gel. A portion of diatomaceous earth equal in size to approximately one-third of the volume of the white gel was added and mixed thoroughly. The gel was then filtered through a 1 in. bed of diatomaceous earth. The solid product was treated by Soxhlet extraction overnight with methanol. The filtrate and extract were combined and reduced in volume by boiling. The volume was doubled with deionized water to aid precipitation. After the solution was allowed to cool, the white precipitate was collected by vacuum filtration and dried overnight in a vacuum desiccator. Yield: 39.5 g (95%), mp 111 °C (lit.[17] 111 °C). ^{1}H NMR (300 MHz, $CDCl_3$ (residual $CHCl_3$ assigned as reference at 7.25 ppm)): δ 2.30 (2H, s, -OH, br), 3.09 (4H, s, -SCH_2CH_2S-), 4.76 ppm (4H, s, benzyl), 7.18−7.42 ppm (8H, m, aromatic).

1,4-Bis(2-formylphenyl)-1,4-dithiabutane. A procedure similar to that of Lindoy and Smith[17] was followed to synthesize 1,4-bis(2-formylphenyl)-1,4-dithiabutane. Dry 1,4-bis(2-(hydroxymethyl)phenyl)-1,4-dithiabutane (10 g) and 70 g of active MnO_2 were suspended in 1000 mL of chloroform. The stirred mixture was refluxed for 8.5

(13) Goodwin, J. A.; Wilson, L. J.; Stanbury, D. M.; Scott, R. A. *Inorg. Chem.* **1989**, *28*, 42−50.
(14) Müller, E.; Bernardinelli, G.; Reedijk, J. *Inorg. Chem.* **1996**, *35*, 1952−1957.
(15) Farnum, D. G.; Rasheed, K. *J. Org. Chem.* **1977**, *42*, 573−574.
(16) Livingstone, S. E. *J. Chem. Soc.* **1956**, 437−440.
(17) Lindoy, L. F.; Smith, R. J. *Inorg. Chem.* **1981**, *20*, 1314−1316.

h. The MnO_2 was removed by filtration through Celite and rinsed twice with 200 mL portions of chloroform. The brilliant pink chloroform solution so obtained was evaporated to dryness, yielding a pink solid that was vacuum dried overnight. Recrystallization from hot ethanol yielded a white solid. Yield: 5.5 g (56%), mp 135−137 °C (lit.[17] 137 °C). ^{1}H NMR (250 MHz, $CDCl_3$ (residual $CHCl_3$ assigned as reference at 7.25 ppm)): δ 3.19 (4H, s, -SCH_2CH_2S-), 7.34−7.88 (8H, m, aromatic), 10.37 (2H, s, -CHO).

[Cu^I(bite)](BF$_4$). 1,4-Bis(2-formylphenyl)-1,4-dithiabutane (0.49 g) and 0.55 g of Cu^{II}(BF$_4$)·4H$_2$O were stirred with 70 mL of *n*-butanol and brought to a boil in an Erlenmeyer flask (note the requirement for a high-boiling solvent.) This resulted in the formation of a greenish-blue suspension. 2,2′-Diaminobiphenyl (0.30 g) was dissolved in 20 mL of *n*-butanol with the aid of slight heating and added to the reaction producing an immediate dark-green color that quickly turned reddish brown. The volume of the solution was reduced to ∼10 mL by boiling. The flask was stoppered and placed in the freezer overnight. The deep orange-red product was collected by filtration, rinsed well with hot toluene, and dried for several hours in a vacuum desiccator. The product was then dissolved in CH_2Cl_2 and filtered. The CH_2Cl_2 was removed by evaporation, and the solid was dried in a vacuum desiccator for several minutes. At this point, the orange-red film was dissolved in methanol and left in a covered beaker for several days until orange-red crystals formed. The crystals were collected by filtration. *Alternative Purification:* Purification by column chromatography was achieved by loading 1.0 g of compound dissolved in 10% more than the minimum necessary volume of dichloromethane onto a 3 in. high × 2 in. diameter column of silica gel eluted with dichloromethane. A yellow band eluted while the product remained at the top of the column. Increasing the polarity of the eluant by slowly introducing methanol caused the elution of two additional yellow bands, followed by the product, which had a leading green edge. This green edge was discarded. Evaporating the product band to dryness, followed by the crystallization procedure described above, resulted in the orange product. Yield: 0.30 g (28%), mp 283−285 °C (dec.). ^{1}H NMR (300 MHz, $CDCl_3$ (residual $CHCl_3$ assigned as reference at 7.25 ppm)): δ 3.43−3.57 (4H, m, -SCH_2-CH_2S-), 7.13−7.84 (16H, m, aromatic), 8.38 (2H, s, -CHN-). Anal. Calcd. for $C_{28}H_{22}N_2S_2CuBF_4$: C, 55.96; H, 3.69; N, 4.66; S, 10.67. Found: C, 56.23; H, 3.70; N, 4.45; S, 10.97.

[Cu^{II}(bite)](BF$_4$)$_2$. [Cu^I(bite)](BF$_4$) (0.18 g) was dissolved in 50 mL of dichloromethane. [NO](BF$_4$) (0.05 g) was added after which the solution was stirred and heated. The color immediately began to darken. After 10 min, another 0.04 g of [NO](BF$_4$) was added to the now brown solution. The solution was allowed to cool for 45 min leading to the formation of a dark-green solid. The product was collected by filtration and air dried. The product was then dissolved in 40 mL of nitroethane and crystallized by vapor diffusion with diethyl ether. The microcrystalline product was collected by filtration and dried in a vacuum desiccator overnight. Yield: 0.04 g (20%). Anal. Calcd. for $C_{28}H_{22}N_2S_2CuB_2F_8$: C, 48.90; H, 3.22; N, 4.07; S, 9.32. Found: C, 48.25; H, 3.50; N, 4.44; S, 9.86.

Crystal Growth. Single crystals of [Cu^I(bite)](BF$_4$) and [Cu^{II}(bite)](BF$_4$)$_2$ were grown as described above.

X-ray Diffraction Data Collections. [Cu^I(bite)](BF$_4$). A crystal was mounted on the end of a glass fiber. The unit cell was determined by centering 24 reflections in the 2θ range from 15 to 29°. Data were collected using the $2\theta - \omega$ scan technique and processed on a computer-controlled four-circle Nicolet R3m/V crystal diffractometer with Mo Kα radiation. Two reflections established as standards were checked routinely for deviations of positions and intensities after every 100 reflections. Lorentz and polarization corrections were performed, as was an absorption correction (based on Ψ scans). Systematic absences uniquely identified the space group as $P2_12_12_1$ (No. 19). A summary of data collection parameters is given in Table 1.

[Cu^{II}(bite)](BF$_4$)$_2$. A green diamond-shaped plate single crystal of [Cu^{II}(bite)](BF$_4$)$_2$, $C_{28}H_{22}N_2S_2B_2F_8Cu$, of approximate dimensions 0.02 × 0.30 × 0.42 mm was mounted on the end of a hollow glass fiber with the plate face approximately perpendicular to the ϕ axis using cyanoacrylate glue. Preliminary examination and data collection were performed using Mo Kα radiation ($\bar{\lambda} = 0.710\ 73$ Å) on an Enraf-Nonius CAD4 diffractometer equipped with a graphite crystal incident beam monochromator and a gas flow liquid nitrogen refrigerated low-temperature device operating at 123 ± 2 K. Cell constants and an orientation matrix for data collection were obtained from a least-squares refinement, based on the setting angles of 25 reflections in the range of 11.8° < 2θ < 35.8°, determined by the computer-controlled diagonal slit method of centering using the SET4 routine. The tetragonal cell parameters and calculated volume are as follows: $a = 11.640(2)$ Å, $c = 39.527(3)$ Å, $V = 5355.6(7)$ Å^3. For $Z = 8$ and fw = 687.78 Da, the calculated density is 1.71 g/cm^3. As a check on crystal quality, ω scans of several intense reflections were measured; the width at half-height was 0.43° with a take-off angle of 2.8°. The systematic absences of *hkl*, $h + k + l = 2n + 1$, *hk*0, $h = 2n + 1$, $k = 2n + 1$, and 00*l*, $l = 2n + 1$ uniquely determine the space group to be the centrosymmetric $I4_1/a$ (No. 88).

Table 1. Summary of Crystal Data and Intensity Collection Parameters

	[Cu^I(bite)](BF$_4$)	[Cu^{II}(bite)](BF$_4$)$_2$
T, K	294	123
formula	$C_{28}H_{22}BCuF_4N_2S_2$	$C_{28}H_{22}B_2CuF_8N_2S_2$
formula wt, amu	600.9	687.8
cryst dimens, mm	0.08 × 0.15 × 0.50	0.02 × 0.30 × 0.42
space group	$P2_12_12_1$	$I4_1/a$
cryst syst	orthorhombic	tetragonal
a, Å	14.739(3)	11.640(2)
b, Å	21.370(3)	
c, Å	8.046(2)	39.527(3)
V, Å^3	2534.4(7)	5355.6(7)
Z	4	8
density, calcd g/cm^3	1.575	1.70
radiation	graphite monochromated Mo Kα ($\lambda = 0.710\ 73$ Å)	
diffractometer	Siemens R3m/V	Enraf-Nonius CAD4
criterion for obsd	$F_o > 4.0\sigma(F_o)$	$F_o > 3\sigma(F_o)$
obsd reflections	2004	1617
ind reflections	2566	2775
μ, mm^{-1}	1.071	1.045
residuals	$R_1 = 0.045$	$R_1 = 0.061$
	$R_2 = 0.048$	$R_2 = 0.063$
goodness of fit	1.52	1.04
data/parameter	6.1	7.1

The data were collected at a temperature of 123 ± 2 K using the $\theta/2\theta$ scan technique. The scan rate was fixed at 4.12°/min (in ω). The scan range (in degrees) was determined as a function of θ to correct for the separation of the Kα doublet; the peak width was estimated to be $0.95 + 0.34(\tan\theta°)$, and an additional 25% above and below this range was collected to ensure adequate background ranges. Data were collected to a maximum 2θ of 52.86° (maximum sin θ/λ of 0.626). The horizontal counter aperture was also adjusted as a function of θ, varying from 2.5 to 2.7 mm; the vertical counter aperture was set at 4.0 mm. The diameter of the incident beam collimator was 1.3 mm, and the crystal to detector distance was 21 cm. For intense reflections, an attenuator was automatically inserted in front of the detector; the attenuator factor was 19.3. A summary of data collection parameters is given in Table 1.

X-ray Crystal Structure Determinations. [Cu^I(bite)](BF$_4$). The structure was solved by direct methods. All computations were performed with SHELXTL PLUS VMX, Release 4.11, 1990 (Siemens Analytical X-ray Instruments, Inc.) based on SHELX (Sheldrick, G. M.). Other atoms were recovered from difference maps calculated after least-squares refinement of the CuS_2 core of the cation. Difference maps indicated that the BF_4^- ion was disordered. We refined a disordered model of two tetrahedrons about the B atom, with a common refined B−F distance and constrained F−F distance (FVAR and DFIX commands in SHELXTL-PLUS), with isotropic temperature factors on each F held equal. The occupancy of the major tetrahedron [F(1)−F(4)] refined to 0.71(1). All non-hydrogen atoms of the cation were ultimately refined anisotropically; the hydrogen atoms were added in calculated positions. The enantiomorph was determined using the method of Rogers.[18]

[Cu^{II}(bite)](BF$_4$)$_2$. A total of 5729 reflections were collected, of which 2775 were unique. As a check on crystal and electronic stability

(18) Rogers, D. *Acta Crystallogr.* **1981**, *A37*, 734.

four representative reflections were measured every 60 min of X-ray exposure. Plots of the intensities of these standard reflections versus time showed no systematic changes over the time of the data collection, and no correction for decay was applied.

Lorentz and polarization corrections were applied to the data. The linear absorption coefficient is 10.45 cm^{-1} for Mo Kα radiation. An empirical absorption correction based on a series of ψ-scans was applied to the data. Relative transmission coefficients ranged from 0.793 to 1.000 with an average value of 0.881. Intensities of equivalent reflections were averaged. The agreement factors for the averaging of the 2688 multiply measured reflections with their respective duplicates were 0.084 based on intensity and 0.059 based on F_o. The relatively high values are due to the large number of unobserved data in the data set resulting from the small sample size.

The structure was solved with the MULTAN[19] direct methods program which revealed the positions of 11 of the 17 unique non-hydrogen atoms of the cation. The other non-hydrogen atoms were located from a subsequent difference electron density Fourier map. All hydrogen atoms could be located from difference electron density Fourier maps calculated after preliminary refinement of the non-hydrogen atoms. The structure was refined by a full-matrix least-squares process where the function minimized was $\sum w(|F_o| - |F_c|)^2$, and the weight w is defined as $w = 4F_o^2\sigma^2(F_o^2) = 1/\sigma^2F_o$. The standard deviation on intensities is defined as follows: $\sigma^2(F_o^2) = [S^2(C + R^2B) + p^2F_o^2]/Lp^2$, where S is the scan rate, C is the total integrated peak count, R is the ratio of scan time to background counting time, B is the total background count, Lp is the Lorentz-polarization factor, and the parameter p (here set to 0.04) is a factor introduced to down-weight intense reflections.

Scattering factors were taken from Cromer and Waber.[20] Anomalous dispersion effects were included in F_c;[21] the values for $\Delta f'$ and $\Delta f''$ were those of Cromer.[22] Only the 1617 reflections having intensities greater than 3.0 times their standard deviation (on F_o) were used in the refinements. The model for the final cycles of refinement assigned anisotropic displacement parameters to the non-hydrogen atoms and included the hydrogen atoms in fixed idealized positions (d[C−H] = 0.95 Å, B[H] = 1.1B[$C_{attached}$]), thus including 195 variable parameters and resulting in a data/variable ratio of 7.1/1. Refinement converged with unweighted and weighted agreement factors of $R_1 = \sum|F_o - F_c|/\sum|F_o| = 0.061$ and $R_2 = (\sum w(F_o - F_c)^2/\sum wF_o^2)^{1/2} = 0.063$, and an estimated standard deviation of an observation of unit weight of 1.04. The highest correlation coefficient was 0.38. The highest peak in the final difference electron density Fourier map was 1.06 $e^-/Å^3$ with an estimated error based on ΔF[23] of 0.14 located near the copper atom. The highest peak not associated with the heavy atoms was 0.56 $e^-/Å^3$. Plots of $\sum w(|F_o| - |F_c|)^2$ versus $|F_o|$, reflection order in data collection, sin θ/λ and various classes of indices showed no unusual trends. All calculations were performed on a VAXstation 3200 using the SDP/VAX program system[24] unless noted otherwise.

Spectroscopy. Electronic spectra were collected on a Hewlett Packard 8452A Diode Array Spectrophotometer in 1 cm matched quartz cuvettes. Solutions 1.0×10^{-5} M in [Cu^I(bite)](BF_4) and 1.0×10^{-4} M in [Cu^{II}(bite)](BF_4)$_2$ were made up volumetrically. Scans were collected in the range of 190−820 nm, with the shorter wavelength limited by the solvent. Far IR spectra were collected for [Cu^I(bite)](BF_4) and [Cu^{II}(bite)](BF_4)$_2$ and compared to those for KBF_4, $NaBF_4$, and [Cu^{II}(en)$_2$](BF_4)$_2$. Data were collected on a Perkin-Elmer 1430 ratio recording infrared spectrophotometer. Compounds were run as their Nujol mulls on CsI plates. The spectrometer was purged with argon gas. The X-band EPR spectrum of a frozen acetonitrile glass of [Cu^{II}(bite)](BF_4)$_2$ was obtained at −170 °C with a Varian E-Line EPR spectrometer. Diphenylpicrylhydrazyl was employed as a field reference. Integration was standardized with respect to a solution of $CuSO_4$ of known concentration. Copper X-ray absorption spectroscopic (XAS) data were collected at the Stanford Synchrotron Radiation Laboratory on beam line 7−3 with the SPEAR ring running at 3.0 GeV and between 60 and 90 mA. Tables S-XIV and S-XV of the Supporting Information detail the data collection and data reduction conditions and parameters. Data reduction generally followed published methods.[25]

Conductivity. Solution conductivity data were collected in dichloromethane using a YSI Model 31 conductivity bridge. A temperature of 25 °C was maintained by a constant temperature bath. Dichloromethane solutions 10^{-5} M in [Cu^I(bite)](BF_4), [Cu^{II}(bite)](BF_4)$_2$, and tetra-*n*-butylammonium tetrafluoroborate ($TBABF_4$) were made up volumetrically. The cell constant was determined to be $\theta = 1.58$ cm^{-1} by using a 0.01 M aqueous solution of potassium chloride to calibrate the conductivity cell.

Electrochemistry. Acetonitrile was refluxed over CaH_2 for 12 h and distilled immediately before use. Solutions were prepared in a solvent fume hood. A stock solution of 2.5×10^{-2} M $NaBF_4$ was prepared and used to create solutions of 10^{-3} M ferrocene and [Cu^I(bite)](BF_4). Cyclic voltammograms were collected using a BAS-100BW electrochemical analyzer. Scans were collected at a rate of 100 mV/s using a standard three-electrode configuration with a 1 mm platinum disc working electrode, Ag/AgCl reference electrode, and platinum wire auxiliary electrode.

Variable-Temperature ^{1}H NMR. ^{1}H NMR spectra were collected as a function of temperature on an IBM/Brüker AF-300 NMR spectrometer. Typically 16 scans were accumulated into 32 K of memory and Fourier transformed. Data were collected from room temperature down to approximately 5 °C above the freezing point of the solvent. Spectra were accumulated at 10 °C intervals. The signals due to residual solvent protons were used as internal chemical shift references, with the CHD_2CN quintet assigned a value of 1.93 ppm, the CHD_2COCD_3 quintet a value of 2.04 ppm, and the $CHDCl_2$ triplet a value of 5.32 ppm.

Electron Self-Exchange Kinetics. Spectra were collected in a manner similar to that used for the variable-temperature ^{1}H NMR experiments described above. Line widths were obtained from the transformed spectra by using the Lorentzian curve-fitting routine available on the IBM/Brüker AF-300 spectrometer. Data were collected as a function of temperature and concentration of the oxidized form of the copper complex. Samples were prepared to maintain a constant ionic strength of μ = 25 mM in acetone-d_6 with $TBABF_4$ as the supporting electrolyte. Ten milliliters of an acetone-d_6 solution was prepared from 60.1 mg of [Cu^I(bite)](BF_4). This stock solution was then used as solvent to prepare solutions A and B. Solution A was prepared by dissolving 14.8 mg of $TBABF_4$ to a volume of 3 mL. Solution B was prepared by dissolving 3.4 mg of [Cu^{II}(bite)](BF_4)$_2$ to a volume of 1 mL. NMR samples were prepared by mixing appropriate aliquots of A and B to achieve the desired concentration of [Cu^{II}(bite)](BF_4)$_2$. Solution B was used immediately after the [Cu^{II}(bite)](BF_4)$_2$ had completely dissolved, and the NMR samples were frozen in liquid nitrogen until just prior to insertion into the spectrometer. This procedure prevented significant decomposition of the somewhat unstable oxidized form of the complex.

Numerical Methods. Calculations were performed with Student Matlab for Macintosh (The Math Works, Inc.) on a Macintosh Performa 400 desktop computer. Inverse relaxation times, $1/T_2$, were determined from the line widths ($\Delta\nu_{1/2}$) simply by multiplying by the constant π: $1/T_2 = \pi\Delta\nu_{1/2}$. First-order rate constants, k, were obtained as the inverse paramagnetic contribution to relaxation time, $1/T_{2p}$, by subtracting the inverse natural relaxation time at a given temperature from the inverse average relaxation time observed, $1/T_2$, in the presence of copper(II): $k = 1/T_{2p} = 1/T_2 - 1/T_{2n}$.

The activation parameters of the self-exchange reaction were determined from Eyring plots. Since

$$k = (\kappa T/h)e^{-\Delta H^{\ddagger}/RT}e^{\Delta S^{\ddagger}/R} \quad (1)$$

the enthalpy, $\Delta H^{\ddagger}$, and the entropy, $\Delta S^{\ddagger}$, of activation may be obtained

(19) Main, P.; Fiske, S. J.; Hull, S. E.; Lessinger, L.; Germain, G.; DeClercq, J.-P.; Woolfson, M. M. *MULTAN 11/82*; University of York: York, England, July 1982.

(20) Cromer, D. T.; Waber, J. T. In *International Tables for X-Ray Crystallography*; The Kynoch Press: Birmingham, England, 1974; Vol. IV, Table 2.2B.

(21) Ibers, J. A.; Hamilton, W. C. *Acta. Crystallogr.* **1964**, *17*, 781.

(22) Cromer, D. T. In *International Tables for X-Ray Crystallography*; The Kynoch Press: Birmingham, England, 1974; Vol. IV, Table 2.3.1.

(23) Cruickshank, D. W. J. *Acta. Crystallogr.* **1949**, *2*, 154.

(24) Frenz, B. A. In *Computing in Crystallography*; Schenk, H., Olthof-Hazelkamp, R., vanKonigsveld, H., Bassi, G. C., Eds.; Delft University Press: Delft, Holland, 1978; pp 64−71.

(25) Scott, R. A. *Methods Enzymol.* **1985**, *117*, 414−459.

from a plot of ln(k/T) versus $1/T$, where T is temperature, R is the gas constant, k is the Boltzmann constant, and h is Planck's constant. Least-squares calculations were weighted with the uncertainty of ln(k/T) for each point.[26]

Results and Discussion

Both of the blue copper proteins plastocyanin (Pc) and Azurin (Az) have been structurally characterized in their Cu(I) and Cu(II) oxidation states.[27−29] In both instances, the major structural difference between the +1 and +2 oxidation states is a slight lengthening of the copper−ligand bonds in the reduced forms. The geometry of the coordination sites in these proteins has been described as a compromise between the preferred geometries of Cu(I) and Cu(II). Vallee and Williams were the first to coin the term entatic[30] in describing the application of Lumry and Eyring's rack mechanism[31] to metalloenzymes. This sterically-imposed entatic state is now frequently cited as the source of the fast self-exchange rates of these proteins, due to the supposed lowering of the enthalpic component of the activation free energy and reduced Franck−Condon barrier.[28,32−34] A fact worth noting, however, is that for at least one measurement of the activation parameters for azurin a favorable entropic component of the activation free energy is implicated as being far more influential than the enthalpic component.[35−37] Furthermore, the literature documents one rather startling example of a four-coordinate small-molecule system ($[Cu^{I/II}((imidH)_2\text{-}bp)_2]^{+/2+}$), which is coordination-number-invariant and thus rather closely mimics the entatic state, yet has one of the slowest self-exchange rates (by NMR line broadening) of any copper redox couple.[5,7]

In a view that challenges the traditional interpretation of the entatic state hypothesis, a recent examination of the electronic structure of the blue copper sites attributes the rapid electron transfer and high redox potential to the favorable configuration of ligand orbitals. Specifically, Guckert *et al.*[38] postulate that the orbitals are arranged such that changes in the ligand−metal orbital mixing are compensated by changes in the orbital energies in a balancing act which results in fairly advantageous electronic configurations in both oxidation states. This view is somewhat at odds with the traditional entatic state hypothesis which postulates that the rigid protein environment enforces an unfavorable geometry on the copper(II) oxidation state. In fact, the authors postulate that an entatic state is enforced upon the copper(I) oxidation state.

Figure 1 displays the ligands for the four CNI copper complexes for which self-exchange rate constant data are available and X-ray structural data are available for both the +1 and +2 oxidation states. We report here for the first time an N_2S_2* (S* designates thioether as opposed to S which designates thiolate) macrocyclic system which is four-coordinate and nearly tetrahedral for the Cu(I) state but which "semi-coordinates" two BF_4^- counterions (in the solid state only; see below) to form an axially elongated octahedral complex for the Cu(II) state, with a surprisingly "flattened" N_2S_2* donor atom set. The synthesis of these $[Cu^{I/II}(bite)](BF_4)_{1,2}$ salts is outlined in Scheme 1. The compounds in Figure 1 are the first copper compounds for which electron-transfer kinetics data have been obtained on systems designed to guarantee both outer-sphere mechanisms and coordination-number-invariance. Although the previously studied five-coordinate open-chain complexes likely operate through outer-sphere mechanisms,[4] the ability of the ligand arms to dissociate leaves some possibility of inner-sphere electron transfer. Such dissociative mechanisms are not available to the present $[Cu^{I/II}(bite)]^{+/2+}$ macrocyclic compounds, virtually eliminating any pathways for inner-sphere electron transfer.

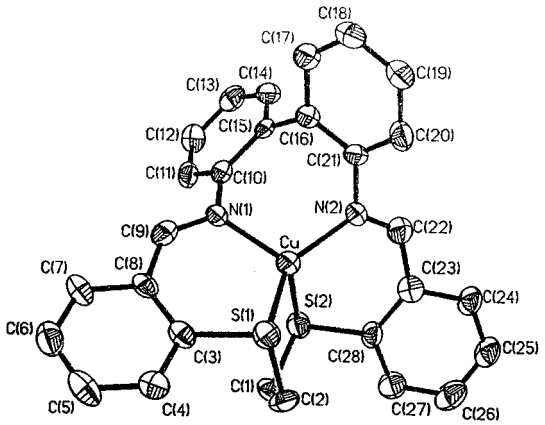

Figure 2. ORTEP drawing of the $[Cu^I(bite)]^+$ cation with the atom labeling scheme. The opposite enantiomorph is shown in order to facilitate comparison with the structure of the Cu(II) analogue.

Scheme 1

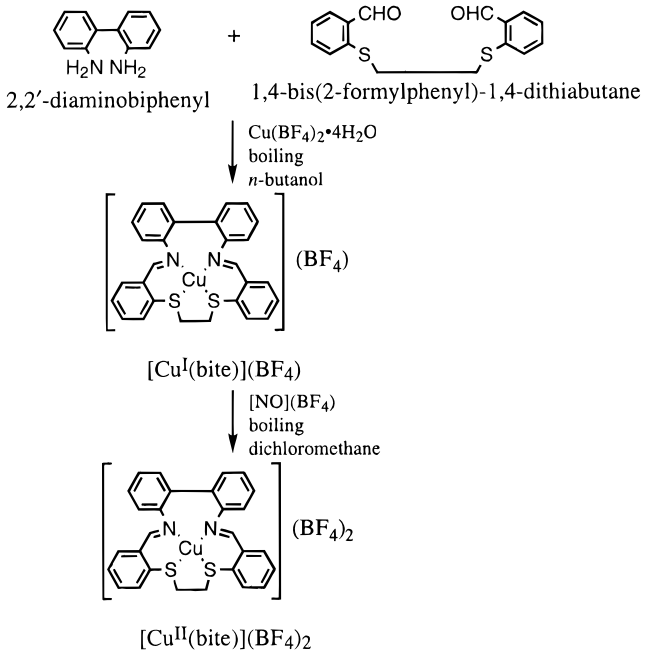

X-ray Crystal Structure Determinations. $[Cu^I(bite)](BF_4)$. An ORTEP structural plot for the $[Cu^I(bite)]^+$ cation is presented in Figure 2, while the bond lengths and angles are given in Tables 2 and 3. The structure consists of separate $[Cu^I(bite)]^+$

(26) Bevington, P. R.; Robinson, D. K. *Data Reduction and Error Analysis for the Physical Sciences*; 2nd ed.; McGraw-Hill, Inc.: New York, 1992.
(27) Guss, J. M.; Harrowell, P. R.; Murata, M.; Norris, V. A.; Freeman, H. C. *J. Mol. Biol.* **1986**, *192*, 361.
(28) Shepard, W. E. B.; Anderson, B. F.; Lewandoski, D. A.; Norris, G. E.; Baker, E. N. *J. Am. Chem. Soc.* **1990**, *112*, 7817−7819.
(29) Guss, J. M.; Bartunik, H. D.; Freeman, H. C. *Acta Crystallogr.* **1992**, *B48*, 790−811.
(30) Vallee, B. L.; Williams, R. J. P. *Proc. Nat. Acad. Sci. U.S.A.* **1968**, *59*, 498−505.
(31) Lumry, R.; Eyring, H. *J. Phys. Chem.* **1954**, *58*, 110−120.
(32) Malmström, B. G. *Eur. J. Biochem.* **1994**, *223*, 711−718.
(33) Gray, H. B.; Malmström, B. G. *Comments Inorg. Chem.* **1983**, *2*, 203−209.
(34) Williams, R. J. P. *J. Mol. Catal.* **1985**, *30*, 1−26.
(35) Groenveld, C. M.; Canters, G. W. *Eur. J. Biochem.* **1985**, *153*, 559−564.
(36) Groenveld, C. M.; Canters, G. W. *Rev. Port. Quim.* **1985**, *27*, 145.
(37) Groenveld, C. M.; Dahlin, S.; Reinhammar, B.; Canters, G. W. *J. Am. Chem. Soc.* **1987**, *109*, 3247.
(38) Guckert, J. A.; Lowery, M. D.; Solomon, E. I. *J. Am. Chem. Soc.* **1995**, *117*, 2817−2844.

Table 2. Bond Lengths (Å) for $[Cu^{I}(bite)](BF_4)$[a]

atom−atom	distance (Å)	atom−atom	distance (Å)
Cu−S(1)	2.194(2)	Cu−S(2)	2.323(2)
Cu−N(1)	1.953(5)	Cu−N(2)	1.938(5)
S(1)−C(2)	1.820(8)	S(1)−C(3)	1.807(7)
S(2)−C(1)	1.828(7)	S(2)−C(28)	1.793(7)
N(1)−C(9)	1.285(8)	N(1)−C(10)	1.426(9)
N(2)−C(21)	1.436(8)	N(2)−C(22)	1.274(8)
C(1)−C(2)	1.501(11)	C(3)−C(4)	1.363(10)
C(3)−C(8)	1.412(10)	C(4)−C(5)	1.417(11)
C(5)−C(6)	1.370(12)	C(6)−C(7)	1.369(11)
C(7)−C(8)	1.407(10)	C(8)−C(9)	1.476(10)
C(10)−C(11)	1.378(10)	C(10)−C(15)	1.415(9)
C(11)−C(12)	1.377(11)	C(12)−C(13)	1.384(11)
C(13)−C(14)	1.410(11)	C(14)−C(15)	1.389(11)
C(15)−C(16)	1.497(10)	C(16)−C(17)	1.404(10)
C(16)−C(21)	1.413(9)	C(17)−C(18)	1.372(10)
C(18)−C(19)	1.384(11)	C(19)−C(20)	1.394(10)
C(20)−C(21)	1.375(9)	C(22)−C(23)	1.468(10)
C(23)−C(24)	1.404(9)	C(23)−C(28)	1.428(10)
C(24)−C(25)	1.354(10)	C(25)−C(26)	1.364(12)
C(26)−C(27)	1.399(10)	C(27)−C(28)	1.368(10)
B−F(1)	1.388(10)	B−F(2)	1.346(10)
B−F(3)	1.370(10)	B−F(4)	1.396(9)
B−F(5)	1.386(15)	B−F(6)	1.368(13)
B−F(7)	1.386(15)	B−F(8)	1.371(17)

[a] Estimated standard deviations are given in parentheses.

Table 3. Bond Angles (deg) for $[Cu^{I}(bite)](BF_4)$[a]

atoms	angle (deg)	atoms	angle (deg)
S(1)−Cu−S(2)	97.8(1)	S(1)−Cu−N(1)	104.6(2)
S(2)−Cu−N(1)	111.6(2)	S(1)−Cu−N(2)	132.5(2)
S(2)−Cu−N(2)	97.8(2)	N(1)−Cu−N(2)	110.6(2)
Cu−S(1)−C(2)	98.0(3)	Cu−S(1)−C(3)	104.7(2)
C(2)−S(1)−C(3)	104.1(3)	Cu−S(2)−C(1)	94.8(2)
Cu−S(2)−C(28)	99.0(2)	C(1)−S(2)−C(28)	104.2(3)
Cu−N(1)−C(9)	123.5(5)	Cu−N(1)−C(10)	114.6(4)
C(9)−N(1)−C(10)	118.8(6)	Cu−N(2)−C(21)	113.2(4)
Cu−N(2)−C(22)	126.4(5)	C(21)−N(2)−C(22)	119.9(6)
S(2)−C(1)−C(2)	115.8(5)	S(1)−C(2)−C(1)	116.1(5)
S(1)−C(3)−C(4)	113.8(5)	S(1)−C(3)−C(8)	124.6(5)
C(4)−C(3)−C(8)	121.0(6)	C(3)−C(4)−C(5)	120.0(7)
C(4)−C(5)−C(6)	120.1(7)	C(5)−C(6)−C(7)	119.5(7)
C(6)−C(7)−C(8)	122.5(7)	C(3)−C(8)−C(7)	116.9(6)
C(3)−C(8)−C(9)	130.4(6)	C(7)−C(8)−C(9)	112.7(6)
N(1)−C(9)−C(8)	128.5(6)	N(1)−C(10)−C(11)	120.2(6)
N(1)−C(10)−C(15)	120.3(6)	C(11)−C(10)−C(15)	119.4(7)
C(10)−C(11)−C(12)	121.9(7)	C(11)−C(12)−C(13)	120.7(7)
C(12)−C(13)−C(14)	117.6(7)	C(13)−C(14)−C(15)	122.6(7)
C(10)−C(15)−C(14)	117.8(7)	C(10)−C(15)−C(16)	125.4(7)
C(14)−C(15)−C(16)	116.7(6)	C(15)−C(16)−C(17)	116.9(6)
C(15)−C(16)−C(21)	126.2(6)	C(17)−C(16)−C(21)	116.4(6)
C(16)−C(17)−C(18)	121.7(7)	C(17)−C(18)−C(19)	121.0(7)
C(18)−C(19)−C(20)	118.7(7)	C(19)−C(20)−C(21)	120.5(7)
N(2)−C(21)−C(16)	118.8(6)	N(2)−C(21)−C(20)	119.4(6)
C(16)−C(21)−C(20)	121.7(6)	N(2)−C(22)−C(23)	126.3(7)
C(22)−C(23)−C(24)	114.5(7)	C(22)−C(23)−C(28)	129.0(6)
C(24)−C(23)−C(28)	116.5(6)	C(23)−C(24)−C(25)	123.0(7)
C(24)−C(25)−C(26)	120.8(7)	C(25)−C(26)−C(27)	118.1(7)
C(26)−C(27)−C(28)	122.7(7)	S(2)−C(28)−C(23)	122.6(5)
S(2)−C(28)−C(27)	118.2(6)	C(23)−C(28)−C(27)	118.9(6)
F(1)−B−F(2)	109.3(7)	F(1)−B−F(3)	109.5(7)
F(2)−B−F(3)	112.8(6)	F(1)−B−F(4)	108.2(6)
F(2)−B−F(4)	109.7(7)	F(3)−B−F(4)	107.2(7)
F(5)−B−F(6)	109.7(11)	F(5)−B−F(7)	108.2(11)
F(6)−B−F(7)	111.4(11)	F(5)−B−F(8)	109.3(11)
F(6)−B−F(8)	110.2(11)	F(7)−B−F(8)	107.9(10)

[a] Estimated standard deviations are given in parentheses.

cations and BF_4^- anions. There are no Cu−F contacts less than 4.0 Å. The coordination about the copper atom is distorted tetrahedral; the Cu−S distances are highly unequal (2.194(2) and 2.323(2) Å). This latter feature of the structure has been reproduced with data sets from three different crystals at widely different times in two different locations! The N1−Cu−S1/N2−Cu−S2, N1−Cu−N2/S1−Cu−S2, and N1−Cu−S2/N2−Cu−S1 dihedral angles are all near the ideal for a tetrahedron (90°) at 78.0(3)°, 76.7(3)°, and 88.9(3)° (av = 81.20(3)°). The interior angles of the tetrahedron range from 97.8(2)° to 132.5(2)° with the average value of 105.4° very near the ideal of 109.5°. The angle between the biphenyl rings is 64.8(3)°. The N1−C9−C8−C3−S1−Cu chelate ring is essentially co-planar with the C3−C8 phenyl ring, while the N2−C22−C23−C28−S2−Cu chelate ring is puckered significantly.

The structure of $[Cu^{I}(bite)](BF_4)$ is unusual primarily for the extraordinarily short Cu^{I}−S(thioether) bond length of 2.194(2) Å, which is the shortest length to date for this type of bond (typically ∼2.3 Å). This distance is much shorter than the Cu−S*(methionine) distance of 2.90 Å found in plastocyanin and is actually much closer to the Cu−S^-(cysteine) distance of 2.13 Å.[39] The extremely tight fit of the ligand about the Cu(I) center may be due to the relatively small cavity of the macrocycle. In fact, in order for Schiff base condensation of this compound to succeed, the rather high boiling point solvent *n*-butanol (bp 118 °C) was required, as the typical solvents used in this kind of reaction (*i.e.*, methanol and ethanol) did not effect closure of the macrocycle. This structure is also the first to be determined for a macrocyclic ligand employing an N_2S_2*(thioether) donor atom set. The molecule is distorted from perfect C_2 symmetry, most notably in the difference in Cu−S bond lengths, but also in the difference in geometry of the N−C−C−C−S−Cu chelate rings in that one is essentially planar while the other is puckered. The source of the distortions from perfect C_2 symmetry is unknown, but may be related to the unusually high redox potential of the $[Cu^{I/II}(bite)]^{+/2+}$ couple (see below). The distortions may also be an effect of crystal packing. A related, nonmacrocyclic, compound has been reported with an N_2S_2 (thiolato) donor atom set, which employs a similar strategy of using a biphenyl-twisted Schiff base;[40] the Cu(II) form of that compound has been reported, but the Cu(I) has not.

The enantiomer reported here is the opposite of the one obtained in the first structure determination of this compound. The compound spontaneously resolves under the conditions of crystallization. The chirality of the present enantiomer with respect to the twist about the C_2 axis is of the Δ configuration.[41] The Cahn−Ingold−Prelog (*R* and *S*) configurations[42] of the biphenyl and copper chiral centers are *R*, while both of the sulfur centers are *S*.

$[Cu^{II}(bite)](BF_4)_2$. An ORTEP structural plot for $[Cu^{II}(bite)](BF_4)_2$ is presented in Figure 3, while the bond lengths and bond angles are given Tables 4 and 5. $[Cu^{II}(bite)]^{2+}$ has crystallographically imposed C_2 symmetry. The dihedral angle between the two N−Cu−S planes of only 3.0° is an extreme degree of flattening when compared to all other coordination compounds employing the biphenyl moiety.[5−7,40,43−45] The presence of two long axial Cu^{II}−F interactions of 2.546(4) Å with BF_4^- gives the structure a resemblance to that of $[Cu^{II}(en)_2](BF_4)_2$, which

(39) Guss, J. M.; Freeman, H. C. *J. Mol. Biol.* **1983**, *169*, 521−563.
(40) Anderson, O. P.; Becher, J.; Frydendahl, H.; Taylor, L. F.; Toftlund, H. *J. Chem. Soc., Chem. Commun.* **1986**, 699−701.
(41) Purcell, K. F.; Kotz, J. C. *Inorganic Chemistry*; W. B. Saunders Company: Philadelphia, 1977; pp 638−644.
(42) Cross, L. C.; Klyne, W. *Pure Appl. Chem.* **1976**, *45*, 11−30.
(43) Cheeseman, T. P.; Hall, D.; Waters, T. N. *J. Chem. Soc.* **1966**, *A*, 1936.
(44) Pignolet, L. H.; Taylor, R. P.; Horrocks, W. D., Jr. *J. Am. Chem. Soc.* **1969**, *90*, 5457.
(45) Frydendahl, H.; Toftlund, H.; Becher, J.; Dutton, J. C.; Murray, K. S.; Taylor, L. F.; Anderson, O. P.; Tiekink, R. T. *Inorg. Chem.* **1995**, *34*, 4467−4476.

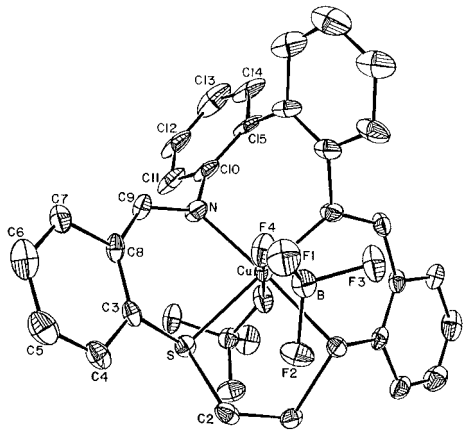

Figure 3. ORTEP drawing of $[Cu^{II}(bite)](BF_4)_2$ with the atom labeling scheme.

Table 4. Bond Lengths (Å) for $[Cu^{II}(bite)](BF_4)_2$[a]

	distance (Å)		distance (Å)
Cu−S	2.286(2)	C9−N	1.273(8)
Cu−N	1.990(5)	N−C10	1.450(8)
Cu−F4	2.546(4)	C10−C11	1.40(1)
S−C2	1.821(7)	C10−C15	1.37(1)
S−C3	1.783(7)	C11−C12	1.38(1)
C2−C2′	1.54(1)	C12−C13	1.39(1)
C3−C4	1.381(9)	C13−C14	1.35(1)
C3−C8	1.397(9)	C14−C15	1.42(1)
C4−C5	1.38(1)	C15−C15′	1.48(2)
C5−C6	1.36(1)	B−F1	1.407(9)
C6−C7	1.38(1)	B−F2	1.345(9)
C7−C8	1.424(9)	B−F3	1.397(9)
C8−C9	1.451(9)	B−F4	1.406(9)

[a] Estimated standard deviations in the least significant digits are given in parentheses. Coordinates of primed atoms are related to those of the corresponding unprimed atoms by the transformation, 1.0 − *x*, 0.5 − *y*, *z*.

Table 5. Bond Angles (deg) for $[Cu^{II}(bite)](BF_4)_2$[a]

	angle (deg)		angle (deg)
S−Cu−S′	89.77(9)	C7−C8−C9	114.9(6)
S−Cu−N	87.4(2)	C8−C9−N	126.7(6)
S−Cu−N′	176.5(2)	Cu−N−C9	125.2(5)
N−Cu−N′	95.4(3)	Cu−N−C10	118.7(4)
S−Cu−F4	91.7(1)	C9−N−C10	116.1(6)
S−Cu−F4′	84.9(1)	N−C10−C11	116.6(7)
N−Cu−F4	93.1(2)	N−C10−C15	120.6(7)
N−Cu−F4′	90.1(2)	C11−C10−C15	122.8(7)
F4−Cu−F4′	175.3(2)	C10−C11−C12	118.5(8)
Cu−S−C2	101.4(2)	C11−C12−C13	120.1(9)
Cu−S−C3	100.3(2)	C12−C13−C14	120.1(8)
C2−S−C3	105.2(3)	C13−C14−C15	122.4(9)
S−C2−C2′	108.4(4)	C10−C15−C14	116.0(8)
S−C3−C4	120.7(5)	C10−C15−C15′	124.3(5)
S−C3−C8	117.8(5)	C14−C15−C15	119.5(6)
C4−C3−C8	120.8(6)	Fl−B−F2	110.2(6)
C3−C4−C5	118.9(6)	F1−B−F3	108.3(6)
C4−C5−C6	121.5(7)	Fl−B−F4	108.0(6)
C5−C6−C7	121.1(7)	F2−B−F3	110.3(6)
C6−C7−C8	118.3(7)	F2−B−F4	111.8(6)
C3−C8−C7	119.3(6)	F3−B−F4	108.2(6)
C3−C8−C9	125.6(6)		

[a] Estimated standard deviations in the least significant digits are given in parentheses. Coordinates of primed atoms are related to those of the corresponding unprimed atoms by the transformation, 1.0 − *x*, 0.5 − *y*, *z*.

has been described as "semi-coordinated" by the BF_4^- anions.[46] Recent structures obtained for related nickel complexes[45] suggest

(46) Brown, D. S.; Lee, J. D.; Melsom, B. G. A. *Acta. Crystallogr.* **1968**, *B24*, 730.

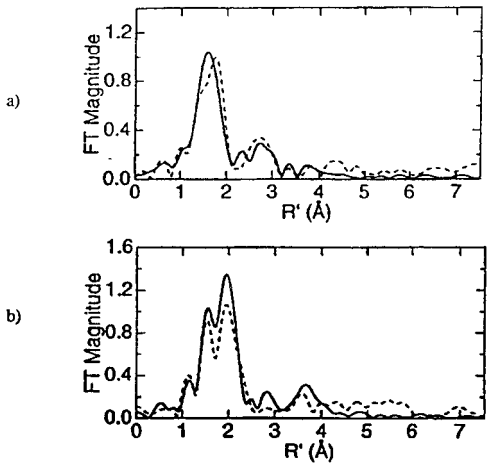

Figure 4. EXAFS FT spectra of solid (—) (30 K) and 1.0×10^{-3} M acetonitrile solution (- - -) (10 K): (a) $[Cu^{I}(bite)](BF_4)$; (b) $[Cu^{II}(bite)](BF_4)_2$.

that the addition of methyl groups to the 6,6′ positions of the ligand (*i.e.*, $[Cu^{II}(biteMe_2)](BF_4)_2$]) would force the copper(II) center into a more tetrahedral configuration, perhaps eliminating ambiguities about the "pseudo-coordinated" anions. However, even for the present $[Cu^{II}(bite)]^{+/2+}$ compound, solution conductivity and EXAFS measurements together imply that the BF_4^- anions are *not* strongly coordinated in solution (see below) where the electron self-exchange studies have been performed.

The crystal is racemic, with both members of the enantiomeric pair present in the unit cell. The configurations of the biphenyl, copper, and sulfur centers for the enantiomer shown in the ORTEP diagram of Figure 3 are all *S*. Comparison of the Cu^{I} and Cu^{II} cations which have identical configurations at the biphenyl moiety illustrates that both sulfur atoms have inverted configuration in the Cu^{II} cation from that found in the Cu^{I} cation. Examination of flexible molecular stick models with (*R*)-biphenyl configuration suggests that square planar Cu^{II} can be ligated fairly strainlessly for both *R,R* and *S,S* configurations of the sulfur atoms. Conversely, similar models containing tetrahedral Cu^{I} results in a highly strained configuration when the sulfur atoms are *R,R* and a much less-strained configuration when they are *S,S*.

EXAFS. $[Cu^{I}(bite)](BF_4)$. The copper K edge spectrum of $[Cu^{I}(bite)](BF_4)$ in the solid state (Figure S-5, Supporting Information) differs slightly from the spectrum obtained in frozen acetonitrile; however, the EXAFS spectra are quite similar as shown in Figure 4a. The position of the K edge confirms the assignment of a formal oxidation state of +1 to the copper center (8984 eV for copper(I) versus 8988 eV for copper(II)). The Fourier transforms (FTs) both exhibit a broad peak with an *R*′ value of approximately 1.6 Å. (Note, *R*′ is not necessarily equal to the radial distance of the scattering atom because the phases are not known independently.) The source of the peak is likely to be the two coordinated nitrogen atoms and the nearest coordinated sulfur atom. The relatively close spacing between the values of the three distances determined by X-ray crystallography (Cu−S(1) 2.194(2) Å, Cu−N(1) 1.953(5) Å, Cu−N(2) 1.938(5) Å) offers an explanation for the lack of resolution in the solid state and the only slight resolution in the solution state. The farthest sulfur atom (Cu−S(2) 2.323(2) Å) is apparently not visible in the FT due to weaker scattering at the larger distance. While the EXAFS and FT data support a strong similarity of the solid and solution state structures for the near coordination sphere, the slight differences observed in the edge spectra suggest a structural difference more removed from the copper atom. Possible explanations may be

the distant coordination of a fifth ligand such as acetonitrile or a less dramatic structural change involving outer solvation of the cation. Conductivity measurements reported below suggest that $[Cu^{I}(bite)](BF_4)$ is a 1:1 electrolyte in CH_2Cl_2 solution which is consistent with the lack of observed fluorine in the solution state FT.

$[Cu^{II}(bite)](BF_4)_2$. The K edge, EXAFS and FT spectra of $[Cu^{II}(bite)](BF_4)_2$ all show very little change upon comparing the solid state and frozen acetonitrile solution data (Figure S-6, Supporting Information). The position of the K edge confirms the assignment of a formal +2 oxidation state to the copper center (8984 eV for copper(I) versus 8988 eV for copper(II)). The absence of a near edge peak at approximately 8980 eV corresponding to a 1s → 3d transition in the solution state spectrum suggests that the complex does *not* undergo a geometry change to tetrahedral upon dissolution, since tetrahedral complexes of copper(II) generally display such a band. Since octahedral and square-planar copper complexes are not known to exhibit well-resolved 1s → $4p_z$ transitions (as would be seen for nickel), the spectrum is consistent with a "pseudo-octahedral" coordination geometry as observed in the solid state and with "pseudo-octahedral" or square-planar geometry in solution. The splitting observed in the first shell FT peak (Figure 4b) is expected, the lower *R*′ peak being mainly due to Cu−N and the higher *R*′ peak being mainly due to Cu−S. The "pseudo-coordinated" fluorine atoms observed at a distance of 2.546(4) Å in the solid state X-ray crystallographic structure are not observed in the FT, most likely due to the long distance and poor scattering ability of fluorine. (Note that the sulfur atom at 2.323(2) Å in $[Cu^{I}(bite)](BF_4)$ is not seen either, despite the shorter distance and stronger scattering ability of sulfur relative to that of fluorine.) The fluorine could well be displaced by acetonitrile nitrogen in the solution state and still be consistent with the observed spectra. Thus, the data are consistent with a variety of solution-state species, including a square-planar complex, a complex weakly bound to BF_4^-, or a complex weakly bound to CH_3CN.

Conductivity. A saturated solution of $[Cu^{II}(bite)](BF_4)_2$ in CH_2Cl_2 (2×10^{-5} M) registered a molar conductivity of 69 cm^2 $equiv^{-1}$ Ω^{-1} as compared to 80 cm^2 $equiv^{-1}$ Ω^{-1} for $[Cu^{I}(bite)](BF_4)$ and 100 cm^2 $equiv^{-1}$ Ω^{-1} for $[(n\text{-}Bu)_4N](BF_4)$ at the same concentrations at 25 °C. $[Cu^{I}(bite)](BF_4)$ and $[Cu^{II}(bite)](BF_4)_2$ in dichloromethane both behave as near 1:1 electrolytes when compared to $[(n\text{-}Bu)_4N](BF_4)$. The solution-state conductivities indicate a substantial degree of dissociation of the "semi-coordinated" BF_4^- counterions (as observed in the solid state) of the Cu(II) molecule in CH_2Cl_2. This may be represented by the equilibrium

$$[Cu^{II}(bite)](BF_4)_2 \rightleftharpoons [Cu^{II}(bite)](BF_4)^+ + BF_4^- \quad (2)$$

Conductivity measurements alone do not allow one to distinguish between a weak ion pair and a coordinated BF_4^- for the species indicated as $[Cu^{II}(bite)](BF_4)^+$. Note that CH_2Cl_2 as a solvent would favor association of $[Cu^{II}(bite)]^{2+}$ with BF_4^- much more strongly than would CH_3CN, because of both the difference in dielectric constants and the difference in their nucleophilicities. Thus, CH_3CN could displace weakly-coordinated BF_4^-, while CH_2Cl_2 would not. The data are consistent with the acetonitrile EXAFS data presented above in that $[Cu^{II}(bite)](BF_4)_2$ may exist in CH_3CN as a free four-coordinate complex, as a loose ion pair with BF_4^-, as a complex weakly coordinated by one BF_4^- anion, or as any of the above with a coordinated CH_3CN ligand.

Electronic Spectroscopy. $[Cu^{I}(bite)](BF_4)$. The UV−vis spectrum obtained in acetone closely resembles that obtained in dichloromethane, with the most notable difference being the cutoff points of the respective solvents (Figure S-3, Supporting Information). However, the spectrum obtained in acetonitrile ($\lambda_{max} \approx 350$ nm; $\epsilon = 8000$ M^{-1} cm^{-1}) is significantly blue shifted with respect to the other two ($\lambda_{max} \approx 400$ nm; $\epsilon = 6000$ M^{-1} cm^{-1}). When interpreted in light of the EXAFS and variable-temperature ^1H NMR data below, this spectral behavior provides some evidence of an interaction between $[Cu^{I}(bite)](BF_4)$ and acetonitrile.

$[Cu^{II}(bite)](BF_4)_2$. The UV−vis spectrum of $[Cu^{II}(bite)](BF_4)_2$ in acetonitrile, as shown in Figure S-4 (Supporting Information), displays a low-energy band at 646 nm not found in the $[Cu^{I}(bite)](BF_4)$ spectrum. This moderately intense band ($\epsilon = 1154$ cm^{-1} M^{-1}) looks quite like a "d−d" transition arising from a distorted square-planar geometry.[47] Other synthetic copper(II) complexes with thioether donors also exhibit low-energy bands of similar intensity.[48] Most likely, these LF bands achieve their enhanced intensity by stealing intensity from an intense $[Cu^{II} \leftarrow S^*$ (thioether)] charge-transfer (CT) band located at higher energy via a vibronic coupling mechanism. In comparison, the band in the spectrum of $Pc(Cu^{II})$ at 595 nm with $\epsilon \cong 4500$ cm^{-1} M^{-1} is thought to arise from a $[Cu^{II} \leftarrow$ S(cysteine)] charge transfer rather than a $[Cu^{II} \leftarrow S^*$(methionine)] transition.[49]

The spectrum obtained in acetone is blue shifted only slightly from that obtained in acetonitrile. In addition, the intensity of each peak is slightly lower in acetone. Since $[Cu^{II}(bite)](BF_4)_2$ decomposes in acetone and acetonitrile if left for extended periods of time (several days), the reduced intensity of the absorptions in acetone may reflect a slightly more rapid decomposition in that solvent. The resemblance of the two spectra suggests that the structure of the compound is likely to be very similar in both solvents, thus coordination by either solvent is improbable.

Far IR Spectroscopy. The presence of two long axial Cu^{II}−F interactions of 2.546(4) Å with BF_4^- (see X-ray data above) gives the structure of $[Cu^{II}(bite)](BF_4)_2$ a striking resemblance to that of $[Cu^{II}(en)_2](BF_4)_2$, which has been described as "semi-coordinated" by the BF_4^- anions.[46] The far infrared spectrum of $[Cu^{II}(en)_2](BF_4)_2$ (nujol mull) contains a weak, symmetry forbidden, BF_4^- absorption at 350 cm^{-1} indicating the "semi-coordination" of a BF_4^- anion.[50] A similar band is observed for $[Cu^{II}(bite)](BF_4)_2$ at 350 cm^{-1}, while the spectrum of $[Cu^{I}(bite)](BF_4)$ contains no such band. These results are consistent with the relative specificity of the Cu−F interactions seen in the X-ray crystal structures.

EPR Spectroscopy. $[Cu^{II}(bite)](BF_4)_2$. Past attention has often focused upon the EPR spectrum of $Pc(Cu^{II})$ which displays an unusually small $A_{||}$ value (0.008 cm^{-1}) compared to simple copper(II) coordination compounds.[51] In this regard, $[Cu^{II}(bite)](BF_4)_2$ gives an undistinguished copper(II) EPR spectrum having $g_\perp = 2.00$, $g_{||} = 2.17$, and $A_{||} = 0.015$ cm^{-1}, with integration of the signal demonstrating that all copper in the sample is EPR active.

Electrochemistry. $[Cu^{I}(bite)](BF_4)$. Although $[NO](BF_4)$ oxidizes $[Cu^{I}(bite)](BF_4)$ by one electron chemically, the compound displays poor electrochemical reversibility. Cyclic voltammetry experiments in CH_3CN show that at lower scan

(47) Styka, M. C.; Smierciak, R. C.; Blinn, E. L.; DeSimone, R. E.; Passariello, J. V. *Inorg. Chem.* **1978**, *17*, 82.
(48) Martin, M. J.; Endicott, J. F.; Ochrymowycz, L. A.; Rorabacher, D. B. *Inorg. Chem.* **1987**, *26*, 3012−3022.
(49) Gewirth, A. A.; Solomon, E. I. *J. Am. Chem. Soc.* **1988**, *110*, 3811.
(50) Brown, D. S.; Lee, J. D.; Melsom, B. G. A.; Hathaway, B. J.; Procter, I. M.; Tomlinson, A. A. G. *J. Chem. Soc., Chem. Commun.* **1967**, 369.
(51) Boas, J. F. In *Copper Proteins and Copper Enzymes*; Lontie, R., Ed.; CRC Press: Boca Raton, FL, 1984; Vol. 1, p 2.

Table 6. Redox Potentials for Pertinent $Cu^{I/II}$ Couples[a]

copper redox pair	reference electrode	solvent	DAS	$E_{1/2}$[b]	ref
$[Cu^{I/II}(2,9\text{-}Me_2phen)_2]^{+/2+}$	SCE	CH_3CN	N_4/N_4O	+0.92	60
$[Cu^{I/II}(bite)]^{+/2+}$	Ag/AgCl	CH_3CN	$N_2S_2*/N_2S_2*(F_2)$	+0.91	TW
$[Cu^{I/II}(Me_2\text{-}2,3,2\text{-}S_4)]^{+/2+}$	NHE	H_2O	S_4*/S_4*O_2	+0.82	48
$[Cu^{I/II}(\text{fungal laccase})]^{+/2+}$		H_2O	N_2SS*	+0.78	61,62
$[Cu^{I/II}([15]aneS_5)]^{+/2+}$	NHE	H_2O	S_4*/S_5*	+0.75	48
$[Cu^{I/II}([14]aneS_4)]^{+/2+}$	NHE	H_2O	S_3*O/S_4*O_2	+0.60	48
$[Cu^{I/II}(\text{plastocyanin})]^{+/2+}$		H_2O	N_2SS*	+0.38	63−65
$[Cu^{I/II}(2,2'\text{-bis}(2\text{-imidH})bp)_2]^{+/2+}$	SCE	CH_3CN	N_4	+0.35	7
$[Cu^{I/II}(\text{stellacyanin})]^{+/2+}$		H_2O	$N_2S(?)$	+0.18	66
$[Cu^{I/II}(py)_2DAP]^{+/2+}$	SCE	CH_3CN	N_5	+0.10	12
$[Cu^{I/II}(imidR)_2DAP]^{+/2+}$	SCE	CH_3CN	N_5	−0.02	12
$[Cu^{I/II}(imidH)_2DAP]^{+/2+}$	SCE	CH_3CN	N_5	−0.03	12
$[Cu^{I/II}((5\text{-MeimidH})_2DAP)]^{+/2+}$	Ag/AgCl	CH_3CN	N_5	−0.12	67

[a] DAS = donor atom set. TW = this work. [b] Potentials are reported relative to NHE. Correction factors of 0.22 and 0.24 V were added to potentials reported versus Ag/AgCl and SCE, respectively, to adjust the values to NHE. This correction ignores unknown solvent junction potentials for results obtained in nonaqueous solvents but should yield qualitatively useful information. Potentials are compared in this manner due to the fact that many of the compounds of interest are not reported versus Fc/Fc^+.

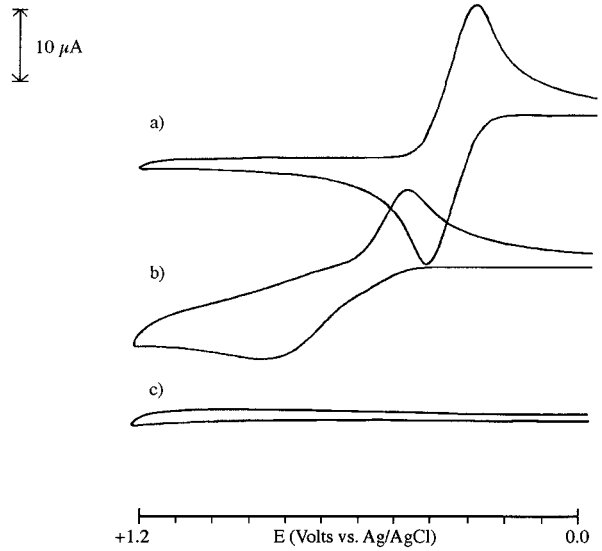

Figure 5. Cyclic voltammograms in CH_3CN (2.5×10^{-2} M $NaBF_4$) at 100 mV/s (Pt button working electrode, Pt wire auxiliary electrode, and Ag/AgCl reference electrode) of (a) ferrocene (10^{-3} M), (b) $[Cu^I(bite)](BF_4)$ (10^{-3} M), and (c) solvent + electrolyte blank.

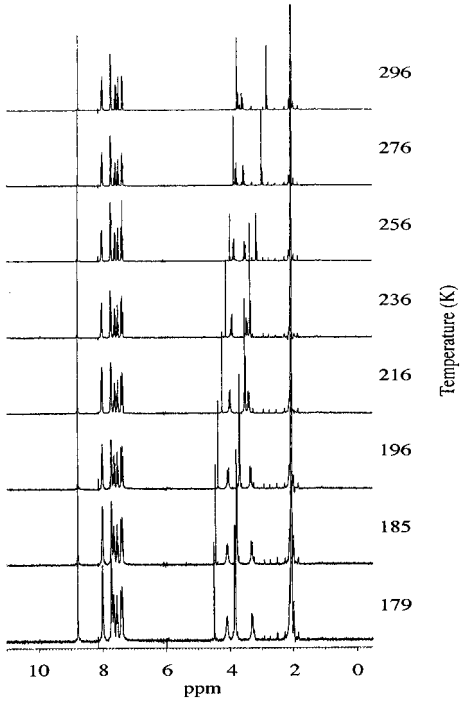

Figure 6. Variable-temperature ^1H NMR (300 MHz) of $[Cu^I(bite)](BF_4)$ in acetone-d_6.

rates, anodic and cathodic peaks develop, but with large peak-to-peak separations (Figure 5). The oxidative peak exhibits pronounced broadening and reduced current intensity with respect to the reductive peak. The $[Cu^{I/II}(bite)](BF_4)_{1,2}$ redox couple shows only quasi-reversible behavior ($\Delta E_{pp} = 0.36$ V) compared to the $Fc^{0/+}$ couple ($\Delta E_{pp} = 0.13$ V) at a scan rate of 50 mV/s. The $E_{1/2}$ of +0.69 V versus Ag/AgCl ($E_{1/2} = +0.34$ for ferrocene under the same conditions) is quite high for a $Cu^{I/II}$ couple (see Table 6), although the large value of ΔE_{pp} introduces some uncertainty into this assessment. The wide peak-to-peak separation and the improved behavior at low scan rates imply sluggish electron transfer at the electrode.

The redox potentials observed for the compounds in this study are compared to those from other systems in Table 6. A unique aspect of the comparison made in the table is that the structures of both the copper(I) and copper(II) forms of all species listed are either known from X-ray crystallography or can be inferred with a high degree of certainty from structures of related complexes. Two trends can be identified in the table. One is the shift toward higher potentials for those complexes having Cu−S(thioether) linkages, which is as expected in view of the strong stabilization of Cu(I) by this soft-binding donor atom. The other trend is for those systems having the higher potentials to have significant structural differences between the two oxidation states, either through a change in coordination number or through some other alteration such as inversion at sulfur (as in $[Cu(bite)]^{n+}$). This tendency emerges despite the rather varied coordination geometries and donor atoms of the various complexes. The trend may reflect the fact that copper(II) is rather strongly destabilized in environments which favor tetrahedral copper(I) and tends to force addition of a fifth ligand upon oxidation. Thus, ligands such as 2,9-dimethyl-1,10-phenanthroline, which strongly favor copper(I), have difficulty accommodating the electronic requirements of copper(II), even after undergoing large geometric distortion to accommodate an additional ligand.

Variable-Temperature ^1H NMR of $[Cu^I(bite)](BF_4)$. Variable-temperature ^1H NMR spectra have been collected in acetone-d_6 (Figure 6), dichloromethane-d_2, and acetonitrile-d_3 (Figures S-7 and S-8, Supporting Information). The spectra obtained for acetone-d_6 and dichloromethane-d_2 are qualitatively very similar. In both cases, very little change is observed in the spectra as the temperature is lowered except for the ethylene signal which appears as a doublet of doublets at low temperature. At higher temperatures, these signals converge to a singlet,

Table 7. ^{1}H NMR Line Broadening Data for $[Cu^I(bite)](BF_4)$ as a Function of Temperature and the Concentration of $[Cu^{II}(bite)](BF_4)_2$: Line Widths (Hz), First-Order Electron Self-Exchange Rate Constants, and Their Standard Deviations[a]

temp (K)	concentration of $[Cu^{II}(bite)](BF_4)_2$ (M)					k_{ex} (s^{-1})	σ_{kex} (s^{-1})
	0.0	0.2×10^{-3}	0.4×10^{-3}	0.6×10^{-3}	0.8×10^{-3}		
235	1.56	1.84	2.40	1.93	1.89	1.4	0.8
255	1.07	2.71	2.25	2.25	2.10	4.0	0.8
275	1.04	4.17	3.97	4.21	4.00	9.6	0.4
295	1.18	7.72	7.84	7.87	8.99	21.7	1.9
315	1.39	14.35	13.99			40.1	0.8
325	1.15	17.86	18.94			54.2	2.4

[a] In acetone-d_6 ($\mu = 25$ mM, $TBABF_4$ electrolyte). Line width is of the imine H^+ resonance at ~8.6 ppm.

although without significant line broadening. The only significant difference of behavior between the two solvents is the convergence temperature for this signal. In dichloromethane-d_2, the splitting pattern converges to a sharp singlet at 287 ± 10 K, whereas in acetone-d_6, convergence appears to lie above 296 K. (Note, the peaks at 3.85 and 4.50 ppm are present in the acetone-d_6 as obtained from the supplier and do not arise from protons on the bite ligand; the peak at 1.50 ppm in dichloromethane-d_2 is due to water.) The behavior at low temperature implies that the ethylene protons exist as two pairs of equivalent nuclei, which indicates that the asymmetry seen in the crystal structure is effectively removed in solution. This could be easily achieved by a rapid oscillation in the two Cu−S bond lengths, leading to effective C_2 symmetry. The high-temperature behavior evidently arises from a temperature-dependent chemical shift, leading to accidental overlap of the two resonances. This could arise from a temperature-dependent conformational equilibrium within the ethylene linkage.

A significantly different situation is obtained in acetonitrile-d_3. The behavior of the ethylene signal appears to be fairly similar to that observed in the other solvents in the range of 288−348 K, with convergence of the signal to a sharp singlet imminent at 348 K. However, below 288 K, the spectrum is dramatically different. All peaks begin to broaden significantly, and the imine signal reaches a coalescence at 248 ± 10 K. By 238 K, the imine pattern has begun to resolve into two broad signals of unequal intensity (Figure S-8, Supporting Information). Once again, this behavior of $[Cu^I(bite)](BF_4)$ in CD_3CN is quite different from that in any other solvent. The splitting of the imine signal at low temperature is most likely due to either (1) coordination of acetonitrile or (2) an equilibrium mixture of two isomers, related, perhaps, by inversion at sulfur. Slow interconversion for either of these processes at low temperature could lead to the observed behavior. Acetonitrile, because of its relatively high dielectric constant, could uniquely support such an equilibrium. Either of these equilibrium explanations would also offer reasonable explanations for the EXAFS and UV−vis spectra already discussed. The lack of any such behavior in acetone and the similarity of the acetone spectra to those obtained in noncoordinating dichloromethane strongly suggest that $[Cu^I(bite)]^+$ remains cleanly four-coordinate in those solvents. For this reason, and because of solubility considerations, acetone-d_6 was selected as the solvent of choice for the electron self-exchange kinetics.

Electron Self-Exchange Kinetics by ^{1}H NMR Line Broadening. The electron self-exchange kinetics in acetone-d_6 was investigated by use of ^{1}H NMR line broadening measurements. For this purpose, the line width of the resonance at ~8.8 ppm arising from the imine protons of $[Cu^I(bite)]^+$ was measured as a function of the concentration of $[Cu^{II}(bite)]^{2+}$ over a range of temperatures. The results are given in Table 7, and they show a rather unusual trend: the first addition of Cu(II) leads to a significant line broadening but subsequent increments in [Cu(II)] lead to no further broadening. This behavior is illustrated in Figure 7. From these results the overall rate law for the electron-exchange process is given simply as

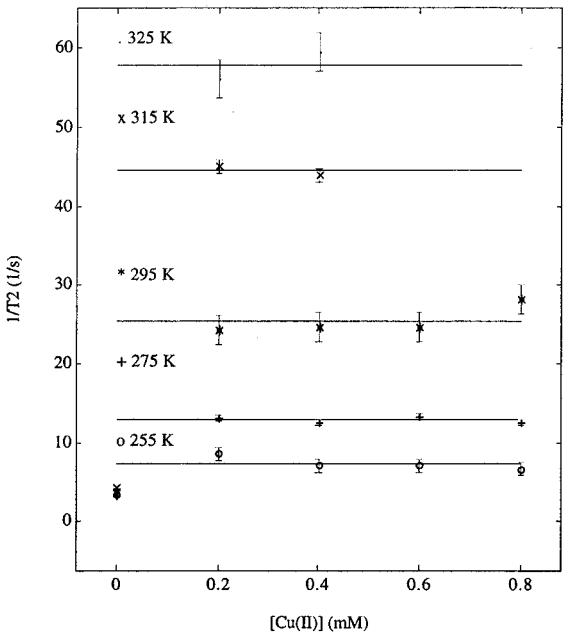

Figure 7. Plot of T_2^{-1} (s^{-1}) versus concentration (mM) of [Cu(II)] for the $[Cu^{I/II}(bite)](BF_4)_{1,2}$ system as function of temperature in acetone-d_6.

$$\text{rate of exchange} = k_{ex}[Cu^I(bite)]^+ \tag{3}$$

Least-squares analysis of the results gives a value of 21.7 (1.9) s^{-1} for k_{ex} at 295 K in acetone-d_6. The activation parameters have likewise been determined to be $\Delta H^{\ddagger} = 23.3(0.7)$ kJ mol^{-1} and $\Delta S^{\ddagger} = -140.8(2.3)$ J mol^{-1} K^{-1}.

In view of the unusual rate law for the electron-exchange process and the X-ray structural evidence for the redox reaction leading to inversion at both sulfur atoms, it is reasonable to think that the mechanism consists of some of the following steps:

$$[Cu(bite)]^+ \rightleftharpoons *[Cu(bite)]^+ \tag{4}$$

$$[Cu(bite)]^{2+} \rightleftharpoons *[Cu(bite)]^{2+} \tag{5}$$

$$[Cu(bite)]^+ + *[Cu(bite)]^{2+} \rightleftharpoons *[Cu(bite)]^{2+} + [Cu(bite)]^+ \tag{6}$$

$$*[Cu(bite)]^+ + [Cu(bite)]^{2+} \rightleftharpoons [Cu(bite)]^{2+} + *[Cu(bite)]^+ \tag{7}$$

$$*[Cu(bite)]^+ + *[Cu(bite)]^{2+} \rightleftharpoons [Cu(bite)]^{2+} + [Cu(bite)]^+ \tag{8}$$

$$[Cu(bite)]^+ + [Cu(bite)]^{2+} \rightleftharpoons *[Cu(bite)]^{2+} + *[Cu(bite)]^+ \tag{9}$$

In this mechanism, steps 4 and 5 are intramolecular isomerization reactions, while steps 6−9 are electron-transfer reactions that preserve the approximate configurations of the reactants. Process 6 can be ruled out, because it would not lead to the observed rate law. Processes 7 and 8 could lead to the observed rate law if prior isomerization of Cu(I) were rate limiting. Process 9 could also be operative if relaxation of the product,

*[Cu(bite)]$^{2+}$, were slow. The molecular-modeling studies described above suggest that isomerization of Cu(I) is unfavorable, which would be consistent with it as the rate-limiting process. On the other hand, relaxation of *[Cu^{II}(bite)]$^{2+}$ could be slow, even if it were less energetically driven than relaxation of *[Cu^{I}(bite)]$^{+}$. Irrespective of whether process 7, 8, or 9 is operative, the derived rate law identifies k_{ex} as k_4.

Rorabacher and co-workers[52,53] have examined numerous cross-exchange reactions of copper systems in which two isomers of copper can be formed in either oxidation state. When cross reactions are performed with simple redox partners that exhibit no such isomerism, the consequence is a mechanistic "square scheme". Note that the scheme in reactions 4−9 is more complex than the square scheme. This arises because both the oxidant and reductant can participate in isomerization reactions. As the Rorabacher group has shown, the square scheme can lead to a variety of complex kinetic behaviors, including first-order kinetics. However, they have never reported a self-exchange reaction that shows first-order kinetics. In this regard, our observations on the [Cu$^{I/II}$(bite)]$^{+/2+}$ system are unique.

An interesting comparison can be made with the [Cu$^{I/II}$(*trans*-cyhx[14]aneS$_4$)]$^{+/2+}$ redox couple.[53] It has been shown by X-ray crystallography that inversion at two of the S atoms accompanies the redox process for this macrocyclic complex. The two atoms undergoing the inversion process are trans to each other in the macrocyclic ring, which thus differs from the [Cu$^{I/II}$(bite)]$^{+/2+}$ system where the two inverting S atoms are cis to each other. Efforts to measure the self-exchange rate constant of the [Cu$^{I/II}$(*trans*-cyhx[14]aneS$_4$)]$^{+/2+}$ redox couple by ^{1}H NMR line broadening were not successful because additions of Cu(II) led to no observable line broadening. This behavior was attributed to a low second-order self-exchange rate constant.[53] We suggest as an alternative explanation that the rate law is actually overall first-order, as seen for [Cu$^{I/II}$(bite)]$^{+/2+}$.

The self-exchange rate constant for [Cu$^{I/II}$(bite)]$^{+/2+}$, 21.7 (1.9) s^{-1} (295 K, acetone-d_6), is difficult to compare directly to rate constants observed for other copper systems, as it appears to be the sole case for which electron self-exchange is truly first order at copper(II) concentrations on the order of 1 mM. The [Cu$^{I/II}$(bite)](BF$_4$)$_{1,2}$ system is only the sixth copper complex for which activation parameters have been determined by the variable-temperature line broadening technique. The enthalpy of activation of $\Delta H^{\ddagger} = 23.3(0.7)$ kJ/mol is fairly high and may be indicative of a Cu−ligand bond breaking/forming process that could occur before electron transfer. One system in which such a coordination number change is known to occur ([Cu$^{I/II}$([15]aneS$_5$)]$^{+/2+}$)[54] was determined to have an enthalpy of activation of only $\Delta H^{\ddagger} = 14(4)$ kJ/mol. The complex is 5-coordinate and square pyramidal in the Cu(II) state and tetracoordinate and pseudotetrahedral in the Cu(I) state.[55] On the basis of the large enthalpic changes expected for a bond breaking/bond forming process, one might predict the self-exchange rate for this small-molecule system to be quite slow. In fact, a measurement has shown that the self-exchange rate constant of $k = 2.2(1.1) \times 10^5$ M^{-1} s^{-1} (25 °C, D_2O) for [Cu$^{I/II}$([15]aneS$_5$)]$^{+/2+}$ exceeds those of all other small-molecule copper systems published to date.[54] Van de Linde *et al.* have suggested that, in fact, the enthalpic contribution to the electron transfer may be much smaller than expected for a bond breaking/forming process. The authors of that study postulate that the Cu^{II}−S bond rupture is a very low-energy process and occurs at a rate of about 4 orders of magnitude faster than electron transfer. Comparison with the activation parameters of [Cu$^{I/II}$(5-MeimidH)$_2$DAP]$^{+/2+}$ reveals that the values for both enthalpy and entropy of activation for the two systems (one CNI, the other non-CNI) are essentially identical.[54] Since the [Cu$^{I/II}$(5-MeimidH)$_2$DAP]$^{+/2+}$ system undergoes no bond breaking or forming, the Cu−S bond which breaks in [Cu^{II}[15]aneS$_5$)]$^{2+}$ must not introduce a large barrier to electron transfer.

Finally, the activation entropy of [Cu$^{I/II}$(bite)](BF$_4$)$_{1,2}$ is extremely negative at $\Delta S^{\ddagger} = -140.8(2.3)$ J mol^{-1} K^{-1}. An explanation for this low entropy of activation in the [Cu^{I,II}(bite)]$^{+/2+}$ system will depend on the mechanism of isomerization of Cu(I) (eq 4). Entropy of activation in blue-copper proteins such as azurin lies at the other extreme, with $\Delta S^{\ddagger} = +96$ (29) J mol^{-1} K^{-1}.[35] This enormous entropy value likely reflects the release of solvent molecules upon approach of two protein molecules, a process for which there is no analogy in small molecules. Thus, caution should be exercised in making casual assessments about the active site (a "small-molecule" CNI site) to overall protein electron-transfer rates.

Conclusions

A combination of results from EXAFS, X-ray crystallography, electronic spectroscopy, NMR spectroscopy, conductivity, and far IR spectroscopy has provided a fairly clear picture of the solution state structures of [Cu^{I}(bite)](BF$_4$) and [Cu^{II}(bite)](BF$_4$)$_2$. In acetonitrile, [Cu^{I}(bite)](BF$_4$) shows unusual behavior, which could be due to a configurational equilibrium or to the binding of an acetonitrile molecule as a fifth ligand, consistent with the known affinity of acetonitrile for copper(I) (*e.g.*, [Cu^{I}(CH$_3$CN)$_4$]$^{+}$).[57] In acetone and dichloromethane, however, no evidence of solvent or anion coordination has been observed. Since copper(I) prefers four-coordinate tetrahedral coordination environments to any other, it is almost certain that a close approximation of the tetrahedral, four-coordinate solid-state structure is present in these two solvents. [Cu^{II}(bite)](BF$_4$)$_2$ may weakly coordinate one BF$_4^-$ anion in the solution state, but the lack of any difference between the UV−vis spectra obtained in strongly coordinating acetonitrile and weakly coordinating acetone suggests that the complex adopts the same structure in both solvents. Thus, a four-coordinate, square-planar geometry is the most likely structure for this complex in solution.

Of the copper couples so far examined, two stand out as especially informative with respect to the question of blue-copper electron transfer, in part because of the macrocyclic nature of their ligands which helps to insure outer-sphere electron transfer. [Cu$^{I/II}$(bite)]$^{+/2+}$ and [Cu$^{I/II}$([15]aneS$_5$)]$^{+/2+}$[54] have both been characterized by X-ray crystallography in *both* the copper(I) and copper(II) forms, and each system offers its own unique insight into copper electron transfer. [Cu$^{I/II}$([15]aneS$_5$)]$^{+/2+}$ offers an interesting look at a system in which the coordination number changes from 5 to 4 upon reduction of the copper(II) to copper(I). Despite this bond breaking process, electron transfer remains fast ($k = 1.9(0.6) \times 10^5$ M^{-1} s^{-1} at 298 K) and the enthalpy of activation is rather low ($\Delta H^{\ddagger} = 14(4)$ kJ/mol). [Cu$^{I/II}$(bite)]$^{+/2+}$ offers an informative comparison, in that, while this complex is almost certainly

(52) Dunn, B. C.; Ochrymowycz, L. A.; Rorabacher, D. B. *Inorg. Chem.* **1995**, *34*, 1954−1956 and references therein.

(53) Salhi, C. A.; Yu, Q.; Heeg, M. J.; Villeneuve, N. M.; Juntunen, K. L.; Schroeder, R. R.; Ochrymowycz, L. A.; Rorabacher, D. B. *Inorg. Chem.* **1995**, *34*, 6053−6064 and references therein.

(54) Vande Linde, A. M. Q.; Juntunen, K. L.; Mols, O.; Ksebati, M. B.; Ochrymowycz, L. A.; Rorabacher, D. B. *Inorg. Chem.* **1991**, *30*, 5037.

(55) Corfield, P. W. R.; Ceccarelli, C.; Glick, M. D.; Moy, I. W.; Ochrymowycz, L. A.; Rorabacher, D. B. *J. Am. Chem. Soc.* **1985**, *107*, 2399−2404.

(56) Rijn, J. v.; Driessen, W. L.; Reedijk, J.; Lehn, J. *Inorg. Chem.* **1984**, *23*, 3584−3588.

(57) Sharpe, A. G. *Inorganic Chemistry*; Longman: London, 1986; p 611.

coordination-number-invariant in acetone, significant geometric reorganization occurs upon electron transfer. Despite being coordination-number-invariant, electron transfer is quite slow, has a high enthalpy of activation ($\Delta H^{\ddagger} = 23.3(0.7)$ kJ/mol) and is a first-order process limited by sulfur inversion. One other system worth careful scrutiny, despite not having a macrocyclic ligand, is $[Cu^{I/II}((1\text{-Meimid})_2bp)_2]^{+/2+}$ (Figure 1).[7] This system exhibits very little geometric change upon reduction of the copper(II) form and is also coordination-number-invariant. It also demonstrates an immeasurably small (by ^{1}H NMR T_1 measurements) electron transfer rate ($k < 1 \times 10^2$ M^{-1} s^{-1} at 293 K).

Taken together, the emerging data suggest that, at least for these particular small-molecule compounds, small reorganizational processes at the copper site do not necessarily promote fast electron-transfer reactions, particularly when one considers the $[Cu^{I/II}((1\text{-MeimidH})_2bp)_2]^{+/2+}$ system which has a small structural reorganization process and yet possesses unmeasurably small electron self-exchange rates.[5−7] Furthermore, the $[Cu^{I/II}([15]aneS_5)]^{+/2+}$ couple clearly demonstrates that a cuproprotein active site need not be coordination-number invariant to promote a fast electron-transfer reaction.[54] The $[Cu^{I/II}(bite)]^{+/2+}$ couple further demonstrates that CNI does not ensure rapid electron transfer either. As a corollary to these latter observations, the blue-copper active sites could exhibit larger reorganization and still be fast. This conclusion is at odds with the traditional entatic state view which typically attributes rapid electron transfer at the blue-copper sites to small structural differences between the copper(I) and copper(II) state.[58] This latter view has become so widely accepted as to even appear in textbook explanations of blue-copper reactivity.[59] Guckert *et al.*[38] and Knapp *et al.*[7] have offered alternative explanations for fast electron transfer in terms of favorable electronic pathways provided by the blue-copper site. The unusual nature of the coordination geometry and ligating atoms of the blue-copper site may have more to do with achieving high redox potentials than with achieving fast electron transfer. The tendency of coordination-number-invariant small-molecule copper couples to display high redox potentials certainly bolsters this point of view. Thus, in a thermodynamic (but not necessarily kinetic) sense, the entatic state view is likely valid since it explains the site geometry as a compromise between factors which stabilize both the +1 and +2 copper oxidation states. Finally, and perhaps most importantly, these studies of coordination-number-invariant (and non-coordination-number-invariant) copper coordination compounds have emphasized that one must exercise extreme care in ascribing properties of the cuproprotein as a whole to the copper active site.

Acknowledgment. This work was supported by the NSF (CHE-9412736 to L.J.W. and D.M.S.) and the Robert A. Welch Foundation (C-0627 to L.J.W.). S.F. thanks the U.S. NIH for a NIGMS Training Grant (GM-08362) at Rice University, and W.R.S. also thanks the U.S. NIH (GM-38401).

Supporting Information Available: Figures S-1 and S-2, stereo packing diagrams for the unit cells of $[Cu^{I}(bite)](BF_4)$, $[Cu^{II}(bite)](BF_4)_2$; Table S-I, fractional coordinates and isotropic displacement coefficients, Table S-II, anisotropic displacement parameters, Table S-III, H-atom coordinates and isotropic displacement parameters, Table S-IV, torsional angles, Table S-V, least squares planes and dihedral angles, and Table S-VI, configuration of chiral centers for $[Cu^{I}(bite)](BF_4)$; Table S-VII, fractional coordinates and isotropic displacement coefficients, Table S-VIII, general atomic displacement parameters, Table S-IX, fractional tetragonal coordinates and isotropic thermal parameters for the fixed hydrogen contributors, Table S-X, root-mean-square amplitudes of atomic displacements of the atoms refined anisotropically, Table S-XI, torsional angles, Table S-XII, least squares planes and dihedral angles, and Table S-XIII, configuration of chiral centers for $[Cu^{II}(bite)](BF_4)_2$; Table S-XIV, X-ray absorption spectroscopy parameters for solid-state $[Cu^{I}(bite)](BF_4)$ and $[Cu^{II}(bite)](BF_4)_2$; Table S-XV, X-ray absorption spectroscopy parameters for solution-state $[Cu^{I}(bite)](BF_4)$ and $[Cu^{II}(bite)](BF_4)_2$; Table S-XVI, self-exchange rate constants for CNI Cu(I/II) couples and coalescence temperatures for their Cu(I) compounds; Figure S-3, electronic spectra of $[Cu^{I}(bite)](BF_4)$ in acetone, acetonitrile, and CH_2Cl_2; Figure S-4, electronic spectra of $[Cu^{II}(bite)](BF_4)_2$ in acetone and acetonitrile; Figure S-5, X-ray absorption spectra, EXAFS, and FTs for solid $[Cu^{I}(bite)](BF_4)$ and in acetonitrile solution; Figure S-6, X-ray absorption spectra, EXAFS, and FTs for solid $[Cu^{II}(bite)](BF_4)_2$ and in acetonitrile solution; Figure S-7, variable-temperature ^{1}H NMR spectra of $[Cu^{I}(bite)](BF_4)$ in CD_2Cl_2; Figure S-8, variable-temperature ^{1}H NMR spectra of $[Cu^{I}(bite)](BF_4)$ with 15 mM $[(CH_3)_4N]BF_4$ in acetonitrile-d_3; Figure S-9, Eyring plot for electron exchange in the $[Cu^{I/II}(bite)]^{+/2+}$ system; Figure S-10, recalculated electron-exchange dependence on [Cu(II)] for the $[Cu^{I/II}((5\text{-MeimidH})_2DAP)]^{+/2+}$ system; Figure S-11, recalculated electron-exchange Eyring plot for the $[Cu^{I/II}((5\text{-MeimidH})_2DAP)]^{+/2+}$ system (43 pages). See any current masthead page for ordering and Internet access instructions.

JA9644034

(58) Williams, R. J. P. *Eur. J. Biochem.* **1995**, *234*, 363−381.
(59) Kaim, W.; Schwederski, B. *Bioinorganic Chemistry: Inorganic Elements in the Chemistry of Life*; Wiley: Chichester, 1994; p 196.
(60) Doine, H.; Yano, Y.; Swaddle, T. W. *Inorg. Chem.* **1989**, *28*, 2319−2322.
(61) Malmström, B. G. In *New Trends in Bio-Inorganic Chemistry*; Williams, R. J. P., DaSilva, R. J. R. F., Eds.; Academic Press: London, 1978; pp 59−78.
(62) Reinhammar, B. R. M. *Biochim. Biophys. Acta* **1972**, *275*, 245−259.
(63) Sykes, A. G. *Adv. Inorg. Chem.* **1991**, *36*, 377−408.
(64) Büchi, F. N.; Bond, A. M.; Codd, R.; Huq, L. N.; Freeman, H. C. *Inorg. Chem.* **1992**, *31*, 5007−5014.
(65) Armstrong, F. A.; Butt, J. N.; Govindaraju, K.; McGinnis, J.; Powls, R.; Sykes, A. G. *Inorg. Chem.* **1990**, *29*., 4858−4862.
(66) Peisach, J.; Levine, W. G.; Blumberg, W. E. *J. Biol. Chem.* **1967**, *242*, 2847−2858.
(67) Coggin, D. K. Ph.D. Dissertation, Rice University, 1990.